FUDMA Journal of Sciences (FJS)
ISSN online: 2616-1370
ISSN print: 2645 - 2944
Vol. 9 No. 11, November, 2025, pp 27 – 31
DOI: https://doi.org/10.33003/fjs-2025-0911-4018

FIRST-PRINCIPLES INVESTIGATION OF THE ELECTRONIC STRUCTURE AND OPTICAL RESPONSE OF Ga_2S_3 AND Ga_2Se_3 CHALCOGENIDES

Nwachuku Doris Ngozi

Department of Physics, University of Delta, Agbor, Delta State, Nigeria.

Corresponding authors' email: doris.nwachuku@unidel.edu.ng

ABSTRACT

Gallium sulfide (Ga_2S_3) and gallium selenide (Ga_2Se_3) vacancy defect binary materials in the monoclinic Cc phase with a four formula units in a unit cell have been investigated within the density functional theory (DFT) framework. DFT (LDA +U), with PAW pseudopotentials in the Abinit (v7.10); plane-wave cut-off of 15 Ha, k-point grid of 4x4x4 were used in the calculations. Both Ga_2S_3 and Ga_2Se_3 were identified as semiconductors, exhibiting direct band gaps at the Γ- point, with values of 2.86 eV ($\pm\, 0.05eV$) and 1.47 eV ($\pm\, 0.05eV$), respectively. These results are in agreement with the experimental values of Ga_2S_3 2.48 eV (Işık et al, 2018) and Ga_2Se_3 1.99 eV (Huang, 2013). Orbital contributions to the DOS reveal that, in Ga_2S_3, the VBM is dominated by S-3s states, whereas the CBM is mainly derived from Ga-4s and S-3p states. In Ga_2Se_3, the VBM arises chiefly from Se-4s states, while the CBM is primarily composed of Ga-3d and Se-4p states. Dielectric response function calculations yielded $\varepsilon_1(0)$ of 4.9 ($\pm\, 0.05$) and 6.0 ($\pm\, 0.05$) for Ga_2S_3 and Ga_2Se_3 respectively. These narrow bandgaps enable efficient absorption in the visible range for solar energy conversion and light-emitting applications. The results offer a theoretical foundation for additional experimental research on these materials. It is recommended that temperature-dependence and optical absorption spectra be investigated using other computational methods to assess optoelectronic applications.

Keywords: Pseudopotential, Dielectric Function, LDA+U, Density of States, Binary Materials

INTRODUCTION

Gallium sulfide (Ga_2S_3) and gallium selenide (Ga_2Se_3) are classified as III–VI semiconductor compounds that have attracted growing interest in recent years because of their distinct electronic and optical characteristics. These compounds crystallize in various structural phases such as cubic, monoclinic, orthorhombic, or hexagonal, and are composed of layered configurations where gallium atoms form covalent bonds with chalcogen elements like sulfur (S), selenium (Se), or tellurium (Te). The extent of cationic vacancies present in these structures often varies based on the specific synthesis conditions employed (Huang et al., 2014; Ho, 2020; Matthew et al., 2023). These materials exhibit predominantly covalent bonding with a degree of ionic character, resulting in structurally stable compounds with anisotropic properties. Such characteristics are essential for their effective use in optoelectronic devices, sensors, photodetectors, solar energy systems, and nonlinear optical technologies (Zheng et al., 2021; Zhou et al., 2019). Ga_2S_3, when integrated with carbon-based materials, has been shown to enhance the stability and cycling performance of anode materials in both lithium-ion and sodium-ion batteries (Meng et al., 2014; Wang et al., 2019). Research indicates that Ga_2S_3 compounds have wide band gap energies between 2.5 and 3.4 eV, typically with direct transitions and high transparency in the visible spectrum, which makes them well-suited for ultraviolet (UV) detection (He et al., 2017). In contrast, Ga_2Se_3 compounds exhibit both direct and indirect band gaps with narrower energy ranges from 1.99 to 2.70 eV, enabling efficient absorption in the visible range and making them ideal for solar energy conversion and light-emitting applications (Huang et al., 2013; Zhou et al., 2019). The nature of the band gaps, whether direct or indirect, depends heavily on the specific phase of the material and is closely related to its crystal structure and stoichiometry (Huang et al., 2013). These variations arise from differences in chemical bonding, where Ga–S bonds typically produce larger energy separations compared to Ga–Se bonds, thereby significantly impacting the electronic and optical behavior of the materials (Işık et al., 2019; Güler et al., 2019; Mathew et al., 2023; Ueno et al., 1999; Ho & Chen, 1999)

The optical band gap has been observed to decrease with rising temperature as a result of electron–phonon interactions (Ueno et al., 1999). This temperature dependence is crucial for evaluating and optimizing device performance under varying operational conditions. Ga_2S_3 is widely acknowledged as a wide-bandgap semiconductor, with thin films grown through experimental methods typically exhibiting a direct band gap close to 3.0 eV, as confirmed by absorption spectroscopy measurements (Ho & Chen, 1999). More recent advancements, such as the use of plasma-enhanced atomic layer deposition, have resulted in the fabrication of stoichiometric crystalline Ga_2S_3 films, where a direct band gap of approximately 3.2 eV was recorded along with an optical transmittance of about 70% (Mathew et al., 2023). These results highlight the high optical quality and potential of Ga_2S_3 for transparent electronic and optoelectronic applications. In another study, Park et al, (2022) successfully synthesized high-crystallinity Ga_2S_3 nanowires on gold-coated silicon substrates using a chemical vapor deposition (CVD) method based on thermal evaporation. Density functional theory (DFT) calculations performed alongside UV-visible absorption and photoluminescence measurements revealed a direct band gap value of 3.0 eV, further supporting the semiconducting nature of Ga_2S_3 in nanostructured forms. Experimental ellipsometry on β-Ga_2S_3 single crystals has also provided valuable insights, with findings indicating a band gap of approximately 2.48 eV. This was determined through analysis of the imaginary part of the dielectric function and the absorption coefficient, reflecting the influence of crystal phase and measurement techniques on optical properties (Işık et al., 2019). Güler et al. (2019) investigated Ga_2Se_3 single crystals using spectroscopic ellipsometry and reported an experimental band gap of approximately 2.02 eV, determined through analysis of the absorption coefficient. The relatively low band gap was

attributed to specific vacancy configurations and defect ordering within the crystal structure. The researchers noted that the observed electronic interband transitions and the extracted critical point energies accurately reflect the intrinsic optical response of Ga_2Se_3. On the theoretical side, Huang et al. (2013) performed first-principles calculations on Ga_2Se_3 to study its defect-related semiconducting properties and vacancy ordering. Their self-consistent Giga-Watts (GW) calculations revealed a direct band gap of 2.56 eV for an ordered zigzag line vacancy structure, and an indirect band gap of 1.99 eV for a straight-line ordered vacancy at 0 K. These findings underscore the critical role of vacancy configuration in determining electronic structure.

The variation in theoretical band gap values for Ga_2Se_3 further emphasizes how computational outcomes are highly dependent on the modeling methodology, including the choice of functional and treatment of defects. Ga_2Se_3 has been characterized as a defect semiconductor, where the presence of ordered gallium vacancies lead to distinct behavior when compared to fully stoichiometric III–VI compounds. Specifically, the material exhibits direct band edge transitions, with emission peaks around 1.85 eV attributed to transitions involving Ga 4s and Se 4p–Ga 4p hybridized states (Ho, 2020). These defects critically influence the optoelectronic properties of the material. In both Ga_2S_3 and Ga_2Se_3, the density of states (DOS) is largely governed by the hybridization of Ga-4s and 4p orbitals with S-3p or Se-4p orbitals, which in turn dictate the formation of the valence band maximum (VBM) and conduction band minimum (CBM). However, the presence of gallium vacancies and other structural defects can introduce localized states within the band gap, which significantly alters carrier transport and optical absorption behavior (Park et al., 2020). Accurate modeling of these materials, therefore, requires careful consideration of both structural and electronic factors. Although experiments report phase- and vacancy-dependent optical gaps for Ga_2S_3/Ga_2Se_3 (Işık, 2019), first-principles GW/hybrid-level treatments that explicitly address vacancy ordering in the monoclinic Cc phase are scarce. Here a systematic DFT+ (LDA+U)/PAW study of the monoclinic defective-sphalerite phase, benchmarked against existing hybrid/GW and ellipsometry data is provided to clarify vacancy-driven electronic/optical trends. The correlation term, U, introduces orbital-dependent potentials that split the occupied and unoccupied states of correlated orbitals, accurately placing the Ga – 3d bands and enhances the bandgap prediction, making the values more accurate and closer to experimental values. In this study, Ga_2S_3 and Ga_2Se_3 vacancy defect binary materials in the monoclinic cc phase with a four formula units in a unit cell was investigated within the density functional theory (DFT) framework. This points to the necessity of bridging the gap between theoretical predictions and experimental results for Ga_2S_3 and Ga_2Se_3. This is particularly important for reliably designing devices that exploit their electronic and optical behaviors under real-world conditions.

Computational Details

The chalcogenide compounds Ga_2S_3 and Ga_2Se_3, which crystallize in a defective sphalerite-type zinc blende structure within the monoclinic Cc phase with space group 9, were investigated through first-principles calculations. Each unit cell of the structure contains four formula units, corresponding to a total of 20 atoms. All computations were carried out using the Abinit (v 7.10) package (Gonze et al., 2002; Gonze et al., 2005), which implements the pseudopotential method within the framework of (DFT). The vacancy is at the (0.25, 0.12, 0.33) 4c Wyckoff site. The study comprised (i) structural optimization, (ii) electronic band structure analysis, (iii) TDOS and PDOS contributions and (iv) dielectric properties, including the real and imaginary parts of the function.

The calculations began with full structural optimization, after which the equilibrium lattice parameters, deformation parameters, and the atomic positions were derived. These optimized structural data were subsequently used for the electronic and optical property calculations. The initial lattice parameters, listed in Table 1, were taken from Madelung (2004). For electronic structure computations, the LDA+U scheme available in Abinit was employed. LDA with a Hubbard U = 2.0 - 4.0 eV was applied to Ga-3d states (Perdew & Zunger, 1981). The U component was varied in the calculations with band-gap sensitivity of ±0.2 eV.

In later calculations, the projector augmented wave (PAW) method was used in conjunction with LDA+U (Omehe & Nwachuku, 2021). PAW datasets from PSLibrary v1.1 were used: Ga.paw (valence: $3d^{10}4s^24p^1$), S.paw ($3s^23p^4$), Se.paw ($4s^24p^4$). Norm-conserving pseudopotentials (NC) for optical calculations were taken from PD v0.4.

The ground-state energy convergence was set to 10^{-10} Ha, with a plane-wave kinetic energy cutoff of 15 Ha (≈418.20 eV). This is so because the convergence threshold on energy and wave-function were sufficient. A shifted 4×4×4 Monkhorst–Pack grid, corresponding to 256 k-points, was used for structural and electronic calculations, while an increased k-point mesh of 500 was applied for the optical property simulations.

Table 1: The Lattice Parameters used in the Calculations

	a(Å)	C(Å)	*x*	*y*	*Z*
Ga_2S_3	3.68	6.02	0.36	0.36	0.216
Ga_2Se_3	5.42	10.83	0.25	0.25	0.125

RESULTS AND DISCUSSION

Electronic Band Structure

The electronic band structures of Ga_2S_3 and Ga_2Se_3 are presented in Figure 1 as energy dispersions along high points of symmetry in the Brillouin Zone (BZ). The plot is energy (eV) against high symmetry point of first BZ, the direction of the plot is in Γ-Y-A-M. For Ga_2S_3 (Figure 1a), both the VBM and CBM are seen at the Γ-point, giving a direct energy gap value of 2.86 eV ($\pm\, 0.05eV$) which confirms its semiconducting nature. This is in agreement with the experimental value of 2.48 eV (Işık et al, 2018). Similarly, the band structure of Ga_2Se_3 (Figure 1b) also shows a direct transition at the Γ-point, with an energy gap value of 1.47 eV ($\pm\, 0.05eV$), indicating that it is also a semiconductor, also in agreement with the self-consistent straight line computational value of 1.99 eV (Huang et al, 2013). However, while some studies identify Ga_2Se_3 as having a direct energy band gap, others report an indirect gap. This discrepancy may arise from variations in the structural phase of the material or from the flatness of its conduction and valence bands.

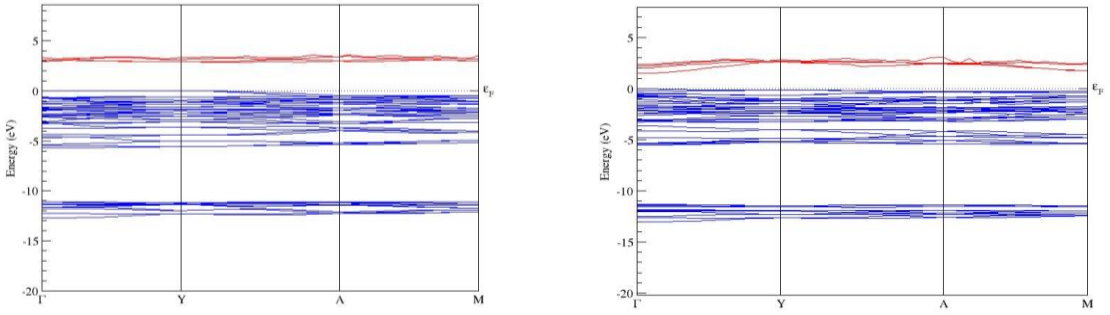

(a) (b)

Figure 1: Electronic band structure of (a) Ga_2S_3 and (b) Ga_2Se_3

In Ga_2S_3 (Figure 1a), the uppermost valence subband has an energy width of 5.8 eV. The intra-valence band gap separating the first and second subbands is 5.2 eV, while the second subband spans an energy range of approximately 1.9 eV. For Ga_2Se_3 (Figure 1b), the top valence subband exhibits an energy width of 5.5 eV, separated from the second subband by a gap of 5.7 eV, with the latter having a width of about 1.8 eV.

Total Density of States (TDOS)

The TDOS for Ga_2S_3 and Ga_2Se_3 are shown in Figures 2a and 2b, respectively, with the DOS plotted against energy (Ha). The peaks in the spectra correspond to orbital contributions that make up the TDOS. For Ga_2S_3 (Figure 2a), the electronic band structure reveals distinct valence subbands separated by intra-valence gaps, with the Fermi level positioned at 0.1 Ha. In the case of Ga_2Se_3 (Figure 2b), the TDOS exhibits sharp peaks and smooth curves that represent the valence subbands, with the Fermi level located at 0.2 Ha. The plots illustrate the contributions of all orbitals, simultaneously reflecting the key features of the band structure.

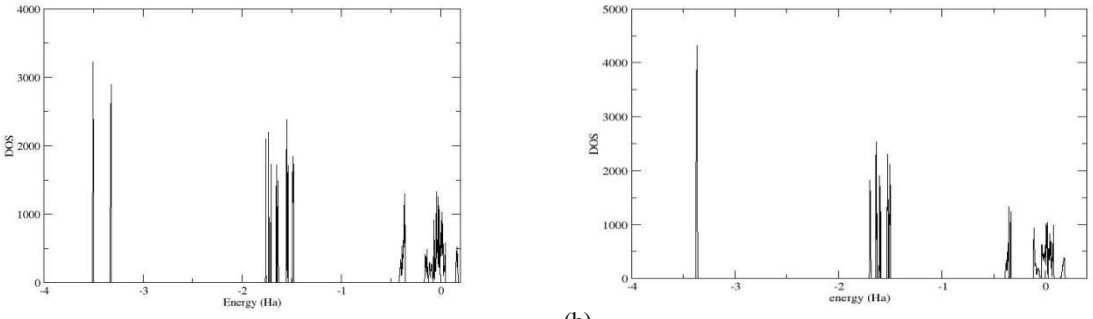

(a) (b)

Figure 2: The Total Density of States for (a) Ga_2S_3 and (b) Ga_2Se_3

Partial Density of States (PDOS) for Ga_2S_3

The PDOS for Ga_2S_3 is presented in Figure 3. The orbital contributions from Ga atoms are shown in Figure 3a: Ga–3p and 4p states are represented in red, Ga–3d in green, and Ga–4s in black. The Ga–3p and 4p states lie at lower energies, concentrated around –3.6 Ha. The Ga–3d states appear as peaks near –1.8 Ha and also extend into the conduction band. The top region of the valence band is mainly formed by Ga–4s and Ga–3d states, which are observed between –0.5 Ha and 0.2 Ha. Figure 3b shows the PDOS contributions from S atoms, where the S–3s states (black) dominate the upper part of the valence band, while the S–3p states (red) appear near –0.2 Ha. Both orbitals overlap into the conduction band. Overall, in Ga_2S_3, the VBM is primarily composed of Ga–3d and S–3s states, whereas the conduction band is mainly from Ga–4s, Ga–3d, S–3p, and S–3s contributions.

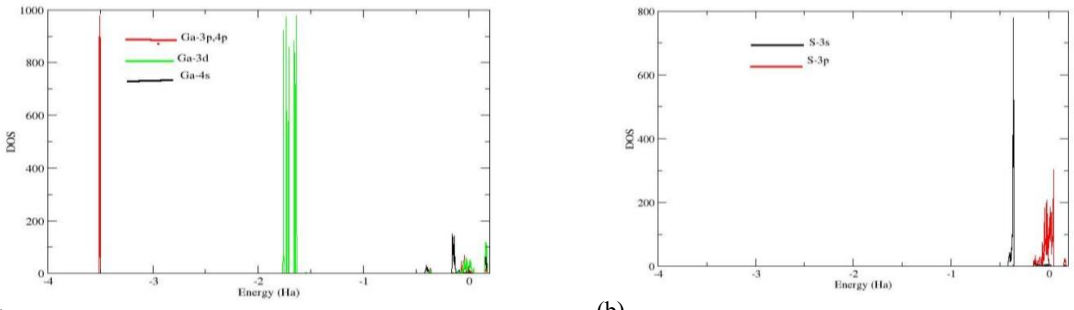

(a) (b)

Figure 3: Partial Density of States for (a) Ga and (b) S

Partial Density of States (PDOS) for Ga_2Se_3

The PDOS for Ga_2Se_3, showing orbital contributions from Ga and Se atoms, is presented in Figure 4. In Figure 4a, the Ga–3p and 4p states are represented in red, Ga–3d in green, and Ga–4s in black. The Ga–3p and 4p states appear at lower energies, concentrated around –3.6 Ha. The Ga–3d states

form distinct peaks near –1.8 Ha and extend into the conduction band. The upper part of the valence band is mainly Ga–4s and Ga–3d states, observed between –0.5 Ha and 0.2 Ha, which is consistent with Ga's contributions in Ga_2S_3. Figure 4b illustrates the Se contributions, with Se–4s states shown in black and Se–4p states in red. The Se–4s orbitals dominate near the top of the valence band around –0.4 Ha, while the Se–4p states contribute prominently as peaks around both the VBM and the CBM, extending partially into the conduction region. In Ga_2Se_3, the VBM is largely composed of Ga–3d and Se–4p states, whereas the conduction band is primarily formed from Ga–4s, Ga–3d, Se–4p, and Se–4s states.

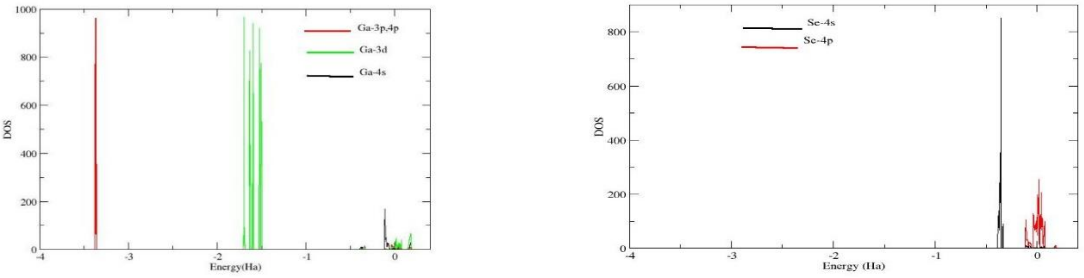

(a) (b)

Figure 4: Partial Density of States for (a) Ga and (b) Se

Optical Property

The dielectric function, ε(ω), which governs the optical response of a material, describes how the material interacts with incident light. Serving as the core parameter of optical behavior, it is a complex function expressed as

$$\varepsilon(\omega) = \varepsilon_1(\omega) + i\varepsilon_2(\omega) \quad (1)$$

Where:

$\varepsilon_1(\omega)$ is the real part and $i\varepsilon_2(\omega)$ is the imaginary part of the dielectric function.

The imaginary part is determined by the joint density of states and the momentum matrix element.

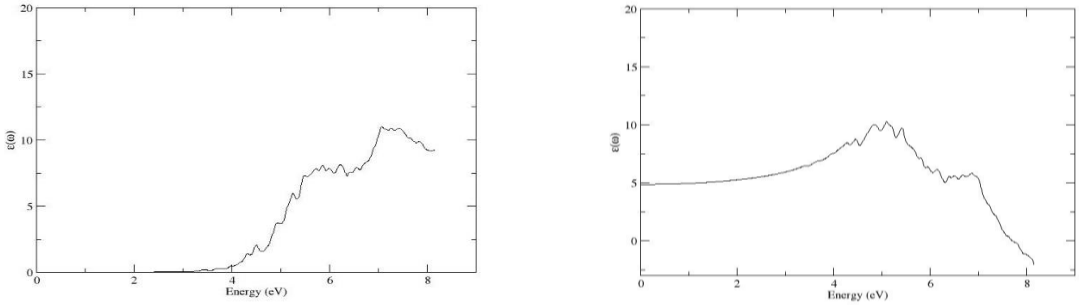

(a) (b)

Figure 5: Plot of the dielectric function for Ga_2S_3 showing (a) Imaginary part and (b) Real part

Figures 5a and 5b present the imaginary and real parts of ε(ω) for Ga_2S_3, respectively. The scissors shift was applied to the computation of the dielectric function. So that the onset of the first peak indicates the energy band gap. The peaks in these spectra correspond to electronic transition points associated with high-symmetry locations in the band structure. Both components of ε(ω) are plotted as a function of photon energy (eV). As shown in Fig. 5a, the first peak appears at the band-edge transition near 7.0 eV. For the real part, which is of more importance, the static dielectric constant $\varepsilon_1(0)$ is approximately 4.9, while the first peak occurs at 5.1 eV with a value of 10.1, as illustrated in Fig. 5b.

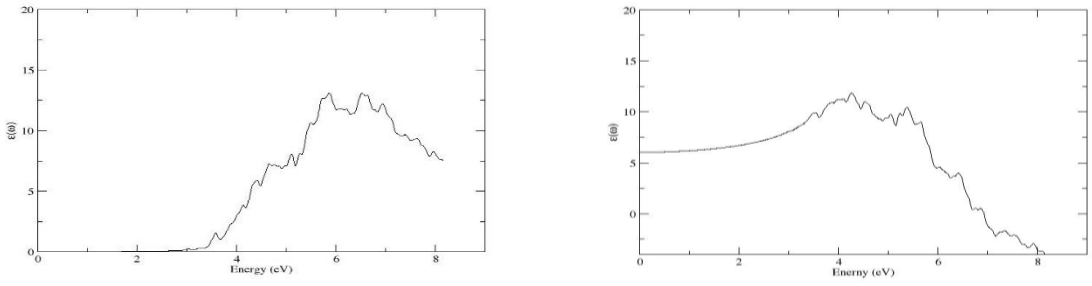

(a) (b)

Figure 6: Plot of the dielectric function for Ga_2Se_3 showing (a) Imaginary part and (b) Real part

Figures 6a and 6b display the imaginary and real parts of the dielectric function, ε(ω), for Ga_2Se_3. The observed peaks correspond to electronic transition points within the material's band structure. For Fig 6a, two peak of about 5.9 eV and 6.6 eV corresponding to the electron transition at the edge of the energy band gap were found. From figure 6b, it is shown that $\varepsilon_1(0)$ for Ga_2Se_3 is about 6.0, with the first peak at 4.4eV corresponding to 10.2 as can be seen in the figure.

CONCLUSION

The structural optimization, electronic band structure, DOS and optical properties of Ga_2S_3 and Ga_2Se_3 were investigated using DFT within the pseudopotential framework and the PAW approach. The LDA+U approach was applied throughout the calculations. the correlation term (U) enhanced the band gap prediction, making the values closer to experimental values. The optimized structural parameters showed good agreement with available experimental data. The results indicate that both compounds are semiconductors. Ga_2S_3 was found to have a direct energy band gap of 2.86 eV (±0.05 eV) in agreement with the experimental value of 2.48 eV (Işık 2018), while Ga_2Se_3 exhibited a narrower direct energy band gap of 1.47 eV (±0.05 eV) in agreement with 1.99 eV self-consistent straight line computation of Huang et al (2013), although they reported indirect band gap. The smaller gap of Ga_2Se_3 enhances absorption in the visible region, making it particularly suitable for solar energy harvesting and light-emitting applications. The calculated static dielectric constants, $\varepsilon_1(0)$, are approximately 4.9 for Ga_2S_3 and 6.0 for Ga_2Se_3. These findings provide a theoretical basis for further experimental exploration of the materials. It is recommended that temperature-dependence and optical absorption spectra be investigated using other computational methods to assess optoelectronic applications.

REFERENCES

Gonze X., Beuken J.-M., Caracas R., Detraux F., Fuchs M., Rignanese G.-M., Sindic L., Verstraete M., Zerah G., Jollet F., Torrent M., Roy A., Mikami M., Ghosez Ph., Raty J.-Y., and Allan D.C., (2002) First-principles computation of material properties: the Abinit software project. *Computational Materials Science*. 25, 478-492.

Gonze X., Rignanese G.-M., Verstraete M., Beuken J.-M., Pouillon Y., Caracas R., Jollet F., Torrent M., Zerah G., Mikami M., Ghosez Ph., Veithen M., Raty J.-Y., Olevano V., Bruneval F., Reining L., Godby R., Onida G., Hamann D. R., and Allan D. C., (2005) A brief Introduction to the Abinit software package. *Z. Kristallogr*. 220, 558-562.

Güler, I., Işıkhan, M., Hasanlı, N., Gasanova, L. & Babayeva, R. (2019). Structural and optical properties of Ga_2Se_3 crystals by spectroscopic ellipsometry. *Journal of Electronic Materials*. 48(4), 2418 – 2422.

He, J., Tian, Z., Wang, Y., & Guo, S. (2017). First-principles study of structural and electronic properties of Ga_2S_3 polymorphs. *Journal of Alloys and Compounds*, *705*, 452–459.

Ho, C. H. (2020). Ga_2Se_3 Defect Semiconductors: The Study of Direct Band Edge and Optical Properties. *ACS Omega,* 5 18527 – 18534.

Ho, C. H., & Chen, H. H. (1999). Optically decomposed near-band-edge structure and excitonic transitions in Ga_2S_3. *Journal of Crystal Growth*, 207(1-2), 69–76.

Huang, G.-Y., Abdul-Jabbar, N. M., & Wirth, B. D. (2013). First Principles Study of the Structure and Band Structure of Ga_2Se_3. *Journal of Physics. Condensed Matter*, 25(22), 225503.

Huang, G.-Y., Abdul-Jabbar, N. M., & Wirth, B. D. (2014). Theoretical study of Ga_2Se_3, Ga_2Te_3 and $Ga_2(Se_{1-x}Te_x)_3$: Band-gap engineering. *Acta Materialia, 71*, 349–369.

Işık, M., Hasanli, N., & Gasanova, L. (2018). Spectroscopic ellipsometry investigation of optical properties of beta-Ga_2S_3 single crystals. *Optical Materials*. 86, 95 – 99.

Işık, M., Hasanli, N., & Gasanova, L. (2019). Optical Properties of (Ga_2Se_3) (0.75) – (Ga_2S_3)(0.25) Single Crystals by Spectroscopic Ellipsometry. *Physica B. Condensed Matter*, 560: 6-10.

Madelung, O. (2004). *Semiconductors: Data Handbook,* Springer, 3rd Edition. 275.

Mathew, F., Poonkottil, N., Solano, E., Poelman, D., & Dendooven, J. (2023). Plasma-enhanced atomic layer deposition of crystalline Ga_2S_3 thin films. *J. Vac. Sci. & Technol.* A41. 060401, 1 – 7.

Meng, X., Libera, J. A., Fister, T. T., Zhou, H., Hedlund, J. K., Fenter, P. & Elam, J. W.(2014). Atomic Layer Deposition of Gallium Sulfide Films using Hexakis (dimethyiamido) digallium and Hydrogen Sulfide. *Chemistry of Materials*. 26(2): 1029 – 1039.

Omehe, N. N., &Nwachuku, D. N. (2021). Electronic Properties of the Chalcopyrites $AgFeS_2$, $AgFeSe_2$ and $AgFeTe_2$ Compounds. *Advanced Material Letters*, 12(1), 21011597.

Park, J., Lee, H., & Kim, D. (2020). Gallium vacancy engineering in Ga_2S_3 for enhanced optoelectronic properties. *Journal of Materials Chemistry C*, *8*, 12315–12322.

Park, K., Kim, D. T., Debela, T. T., Boujnah, M., Zewdie, G. M., Seo, J., Kwom, I. S., Kwak, I. H., Jung, M., Park, J. & Kang, H. S. (2022). Polymorphic Ga_2S_3 nanowires: Phase-controlled growth and crystal structure calculations. *Nanoscale Advances, 4*(15), 3218–3225.

Perdew, J. P. & Zunger, A. (1981). Self-Interaction Correction to Density-Functional Approximations for Many-Electron Systems. *Physical Review B*, 23(10), 5048 – 5079.

Ueno, K., Kawayama, M., Dai, Z. R., Koma, A., & Ohuchi, F. S. (1999).Growth and Characterization of Ga_2Se_3/GaAs (100) Epitaxial Thin Films. *Journal of Crystal Growth, 207*, 69–76.

Wang, K., Ye, W., Yin, W., Chai, W., Rui, Y. & Tang, B. (2019). A Novel Carbon-Coated Ga_2S_3 Anode Material derived from Post-Synthesis Modified MOF for High-Performance Lithium Ion and Sodium Ion Batteries. *Electrochim Acta*. 322: 134790

Zheng, Y., Tang, X., Wang, W., Jin, L. & LI. G. (2021). Large-Sized Ultrathin a- Ga_2S_3 Nanosheets toward High-Performance Photodetection. *Advanced Functional Materials*, 31(6): 2008307

Zhou, Y., Liu, Q., Yan, Y. (2019). Band structure engineering of Ga_2Se_3 for high-performance photovoltaics. *Advanced Materials*, *31*(2), 1805522.